Supporting Information

Controlling the Nucleation and Growth of ultrasmall Metal Nanoclusters with MoS_2 Grain Boundaries

Yongliang Shi,[abc+] Muztoba Rabbani,[d+] Álvaro Vázquez-Mayagoitia[e], Jin Zhao,[cfg] and Wissam A. Saidi[*d]

[a]Center for Spintronics and Quantum Systems, State Key Laboratory for Mechanical Behavior of Materials, School of Materials Science and Engineering, Xi'an Jiaotong University, Xi'an, Shaanxi 710049, China

[b]State Key Laboratory of Surface Physics and Department of Physics, Fudan University, Shanghai, 200433, China

[c]ICQD/Hefei National Laboratory for Physical Sciences at the Microscale, and CAS Key Laboratory of Strongly-Coupled Quantum Matter Physics, and Department of Physics, University of Science and Technology of China, Hefei, Anhui 230026, China

[d]Department of Mechanical Engineering and Materials Science, University of Pittsburgh, Pittsburgh, Pennsylvania 15261, United States

[e]Computational Science Division, Argonne National Laboratory, Lemont, IL, US, 60439

[f]Department of Physics and Astronomy, University of Pittsburgh, Pittsburgh PA 15260, United States

[g]Synergetic Innovation Center of Quantum Information & Quantum Physics, University of Science and Technology of China, Hefei, Anhui 230026, China

+ These authors contributed equally

* Correspondence to: alsaidi@pitt.edu

Computational details

We employ an adaptive genetic algorithm (AGA)[1-3] to explore the structures of Pt nanocluster (NCs) on MoS_2 GBs. AGA combines the accuracy of first-principle calculations and fast structure exploration using auxiliary classical potentials in an iterative way. In the classical GA part, we employ the embedded atom method (EAM)[4, 5] as an auxiliary force field, which is implemented in Large-Scale Atomic/Molecular Massively Parallel Simulator (LAMMPS) code.[6] To get the initiating force field, we initial the EAM force filed by fitting static first-principle results of 12 random structures. And we explore the most energy favorable NPs by iterating it for 200 generations with a pool containing N_P=144 structures. In each generation, we choose $N_p/4$ structure pairs in the pool randomly as parents to generate $N_p/4$ child structures by the mating operator, and we remove duplicated structures to keep the diversity of the structure after optimizing. Duplicated structures are judged by comparing their bond table. In the potential fitting part, 12 lowest-energy structure from classical GA is calculated by DFT to get energies and forces. And then, force matching method,[7, 8] which is implemented in the POTFIT code, is employed to adjust the EAM potential with DFT energies and forces. In the output part, after 20 Iterations, we collect all the structures with DFT energy and optimize 20 lowest-energy structures at a first-principle stage after removing duplicated structures.

The first-principle DFT calculations are carried out within the Perdew-Burke-Ehrenzhof (PBE)[9] exchange-correlation functional and projector augmented wave (PAW) pseudopotentials[10, 11] as implemented in the Vienna Ab initio Simulation Package (VASP) package. The GB substrate used to load Pt atoms and clusters is shown in Fig 1b in the main text. The integration over the Brillouin zone is limited to the Γ point only, as we adopt a relatively large supercell. We used 10 Å in the direction perpendicular to the slabs in conjunction with the dipole correction to mitigate fictitious interaction between periodic images.

The binding energy per atom is defined as,

$$E_{BE} = \frac{1}{\mathrm{n}}\left(E_{GB+Pt_n} - E_{MoS_2} - \mathrm{n}E_{Pt}\right), \tag{1}$$

where $E_{MoS_2+Pt_n}$ is the energy of the Pt_n/GB heterostructure in the optimum geometry, E_{GB} is the energy of the GB substrate, and E_{Pt} is the energy of an isolated Pt atom with two unpaired electrons according to Hund's rules.

To gain further insight into the metal−metal vs. metal-slab stabilizing interactions, we partition the binding energy as follows:

$$E_{BE} = \Delta E_{MoS_2} + \Delta E_{Pt_n} + \Delta E_{MS}. \tag{2}$$

Here, the first term ΔE_{MoS_2} (positive) is the MoS_2 deformation energy, defined as the energy penalty to deform MoS_2 into the structure adopted in the bonding configuration. The second term ΔE_{Pt_n}(negative) measures the energy gain due to the metal−metal bonds and is defined as

$$\Delta E_{Pt_n} = \frac{1}{n}\left(E_{Pt_n} - nE_{Pt}\right) \quad (3)$$

where E_{Pt_n} is the energy of the metallic nanocluster in the frozen geometry adopted on the MoS_2 slab. As we did in our previous study, for consistency E_{Pt_n} is computed with spin-averaged calculation while the monomer reference energy E_{Pt} is computed with spin polarization. Because of this convention, we can see in Table 1 that ΔE_{Pt_1}=0.1 eV even though there is no metal−metal interaction. Using equations 1, 2, and 3, we can define the metal−substrate energy E_{MS} (negative), which measures the interaction between the metal and the substrate. All energy terms in eq 2 are normalized with respect to the number of Pt atoms in the cluster except ΔE_{MoS_2}, which is chosen to be independent of the metal cluster size. As shown in Table S1 and Table S2, ΔE_{MoS_2} is relatively small and thus this choice has a small effect on the results.

The Nudged Elastic Band (NEB) method,[12, 13] used to determine the minimum energy path between initial and final configurations, was used to evaluate the value of energy barriers. The climbing image NEB (CI-NEB) method was applied to a discretized path of 6-13 images. In the CI-NEB,[14, 15] one image is set free from the spring force, maximizing its energy and forcing itself to the exact saddle point. We calculated the reaction barrier as the difference between the saddle points and initial configurations. All the atoms of intermediate NEB images are relaxed, while atomic structures of initial and final configurations are permanently fixed in NEB calculations.

To investigate the electronic/geometric origin of the defect-induced growth mechanism, we performed comprehensive bond analysis using the LOBSTER package[16]. LOBSTER allows extracting precious bonding information from the plane-wave electronic wavefunctions by mapping onto a local basis.[17]

The crystal orbital overlap population (COOP) reveals the bonding and antibonding interaction to the electronic structure by identifying positive and negative orbital overlaps.[18] Integrated COOP (iCOOP) with all occupied energy levels supply a clear bonding and antibonding definition for chemical bonds. Further crystal-orbital Hamiltonian population (COHP)[19] method also provide valuable information as a bond strength indicator in energy contribution by integrating COHP up to Fermi level (thus integrated COHP or iCOHP).[20] The COHP can be taken as the bond-weight density of states, and the COHP value of bonding and antibonding contributions are positive and negative, respectively. Integration over all occupied levels that is iCOHP, roughly provides bond contributions to band-structure energy.

Table S1. Total Binding Energies E_{BE} for Pt_n cluster. Decomposition of E_{BE} into ΔE_{MoS_2}, ΔE_{Pt_n} and ΔE_{MS} as defined in eq 2 is also listed. All energies are normalized by the number of Pt atoms except ΔE_{MoS_2} (see text). Average bond lengths $\bar{l}$ are computed with a threshold of 3 Å.

Configuration	E_{BE}	ΔE_{MoS_2}	ΔE_{Pt_n}	ΔE_{MS}	Pt-Mo	Pt-S	Pt-Pt
			Pt_1				
h-$\perp_7$	-4.57	1.17	0.1	-5.84	2.66	2.43	-----
s-S_2	-3.28	2.06	0.1	-5.44	2.77	2.49	-----
t-Mo_3	-2.94	0.50	0.1	-3.53	2.69	2.32	-----
t-Mo_2	-2.75	0.58	0.1	-3.44	2.77	2.31	-----
			Pt_2				
h-$\perp_7$-t-Mo_3	-4.06	2.30	-1.23	-3.98	2.67	2.49	2.70
h-$\perp_7\perp_5$	-4.05	1.43	-1.29	-3.47	2.73	2.45	2.63
h-$\perp_7$-t-Mo_2	-3.97	1.51	-1.32	-3.41	2.72	2.53	2.64
			Pt_3				
h-$\perp_7$-t-Mo_2-S_3	-4.02	3.97	-1.60	-3.74	2.73	2.37	2.71
h-$\perp_7$-t-$(Mo_2)_2$	-4.00	2.43	-2.36	-2.66	2.73	2.49	2.67
h-$\perp_7$-t-$(Mo_2)_3$	-4.99	3.90	-1.66	-3.63	2.68	2.50	2.71

Table S2. Total Binding Energies E_{BE} for Pt_n cluster on 5|7 grain boundary. Decomposition of E_{BE} into ΔE_{MoS_2},ΔE_{Pt_n} and ΔE_{MS} as defined in eq 2 is also listed. All energies are normalized by the number of Pt atoms except ΔE_{MoS_2} (see text). Average bond lengths $\bar{l}$ are computed with a threshold of 3 Å.

configuration	E_{BE}	ΔE_{MoS_2}	ΔE_{Pt_n}	ΔE_{MS}	Pt-Mo	Pt-S	Pt-Pt
Pt_4	-4.11	5.80	-2.11	-3.44	2.70	2.50	2.59
Pt_5	-4.09	1.85	-2.67	-1.79	2.75	2.41	2.68
Pt_6	-4.10	2.35	-2.85	-1.65	2.75	2.43	2.71
Pt_7	-4.13	2.72	-2.98	-1.53	2.81	2.36	2.61
Pt_8	-4.12	2.36	-3.05	-1.37	2.76	2.42	2.64
Pt_9	-4.18	2.66	-3.30	-1.17	2.81	2.45	2.70
Pt_{10}	-4.18	0.68	-3.37	-0.87	2.75	2.29	2.68
Pt_{11}	-4.19	2.85	-3.43	-1.02	2.82	2.48	2.66
Pt_{12}	-4.23	0.87	-3.52	-0.79	2.91	2.30	2.70
Pt_{13}	-4.30	0.88	-3.56	-0.81	2.89	2.30	2.68
Pt_{16}	-4.31	1.92	-3.57	-0.85	2.69	2.31	2.71
Pt_{20}	-4.44	1.22	-3.85	-0.65	3.00	2.26	2.71

Table S3. Total Binding Energies ΔE_{BE} for Pt_n cluster on 4|6 and 5|8|5 grain boundary. Decomposition of ΔE_{BE} into ΔE_{MoS_2}, ΔE_{Pt_n} and ΔE_{MS} as defined in eq 2 is also listed. Average bond lengths $\bar{l}$ are computed with a threshold of 3 Å.

configuration	ΔE_{BE}	ΔE_{MoS_2}	ΔE_{Pt_n}	ΔE_{MS}	Pt-Mo	Pt-S	Pt-Pt
Pt_1 @ 4|6	-4.75	0.91	0.1	-5.75	2.64	2.42	-----
Pt_1 @ 5|8|5	-6.99	0.79	0.1	-7.88	2.52	>3	-----

Interaction between Pt nanoclusters and MoS_2 grain boundary

In the dimer configuration, we notice an increase in the binding energy. In the Pt_2 configuration with one Pt atom at Mo_3 site decreases the binding energy per atom of Pt_1 h-$\perp_7$ by 0.51 eV. Pt atom on t-Mo_3 is not bonded with the Mo atom strongly. It also decreases the bonding between the hollow site Pt atom and the substrate, thus weakening the metal-substrate interactions. We can see that metal substrate interaction energy ΔE_{MS} increases from -5.84 eV to -3.98 eV. These significant changes indicate that metal-substrate interaction has been affected negatively with the second Pt atom. This sudden ΔE_{MS} jump is also noticed with Pt_5 of -3.44 eV to -1.79 eV when the 2D configurations changes to 3D configurations indicating metal-substrate interaction became weaker.

To better understand, we analyzed the interaction energy between Pt atoms ΔEPt and Pt-substrate interaction energy ΔE_{MS}. With the increasing cluster size, the value for ΔE_{Pt} is decreasing, and for ΔE_{MS} is increasing. The low value of ΔE_{Pt} indicates strong Pt-Pt interactions caused by the more considerable Pt cohesive energy, and because of this energy, Pt atoms take the 3D configurations. This also affects the higher binding energy. Thus, one cannot say whether Pt-Pt interaction or Pt-S interaction dictates the binding energy in these relatively large clusters (5<n<20). We would rather say for large clusters that Pt-Pt and Pt-S interaction dominates the binding energy while in small clusters with $n < 5$, this is caused by Pt-Mo atoms interaction.

The interaction of Pt atoms with substrate atoms deforms the MoS_2 substrate. We introduce ΔE_{MoS2} defined as the substrate's deformation energy difference in the binding configuration with respect to the original substrate. Unlike the case of the pristine surface where ΔE_{MoS2} is negligible small < 0.6 eV for clusters with n < 20, we find that this energy is larger for the GB case indicating the cluster significantly distorts the MoS_2 substrate. For instance, in the second stable configuration of Pt_1, one S atom of GB interchanges its position with hollow site Pt atom, which incurs a 2.06 eV deformation energy of the substrate. In monomer at h-$\perp_7$ configuration, the bond between all atoms in the 7 fold ring have been highly affected: Mo_3-S_3 length increased by 0.23Å, Mo_3-Mo_3 increased by 0.16Å from free standing GB. This can also be judged for the 2D structures (Pt_n<Pt_5), where ΔE_{MoS2} is relatively higher than for the 3D structures, which indicates that with larger clusters, the metal-substrate interaction is getting weaker and thus, deformation of the substrate is also getting negligible.

GB's unique effect is by far has proven to be very different from the pristine surface, but it has a limit. We noticed the hollow site being unoccupied at Pt_{10}, and also, the bond length and bond coordination changed their pattern around that size. However, another interesting fact is that Pt atoms were distributed around 7-fold ring rather than 5-fold ring till Pt_{10}, and the lower layer Pt atoms are not bonded with any substrate atoms from the pristine surface. Only after Pt11 the NCs atoms have been spotted to have a bond with the pristine surface atoms. After Pt_{12}, bonding nature tells, the clusters can not distinguish between the GB and the pristine sites. And Pt_{16}, Pt_{20} clusters Pt atoms are bonded with 5 fold ring's atoms too. This indicates our 5|7 GB's unique effect of developing stable configuration is diminished at larger clusters. The binding energy difference for Pt_{12} and Pt_{13} between GB to the pristine surface is 0.1 eV, and for larger structures, Pt_{16} and Pt_{20}, this difference gets even lower(0.05 eV). Therefore, for small clusters, we can expect much more resistance to the GB's sintering effect, and because of a large number of bonds and higher bond strength, GB should exhibit higher creep resistance than any GB without NC.

Examining the charge decomposition, we find that Pt NCs can accept more charge from MoS_2 GB than from pristine MoS_2. For example, for the monomer case, h-$\perp_7$ accept 0.43 electron due to directly bonded to Mo pair while t-Mo configuration on pristine MoS2 donates electrons to the substrate. As the NCs grow, there is less charge transfer from MoS_2 to Pt. For Pt_3 and Pt_7, NCs accept 0.37 and 0.27 electrons from GB, respectively. On the pristine MoS_2, as the NCs grow, there is more charge transfer from MoS_2 to the metallic NCs. For charge analysis above, we expect ultra-small metallic NCs with higher catalyst activity on GBs than pristine MoS_2.

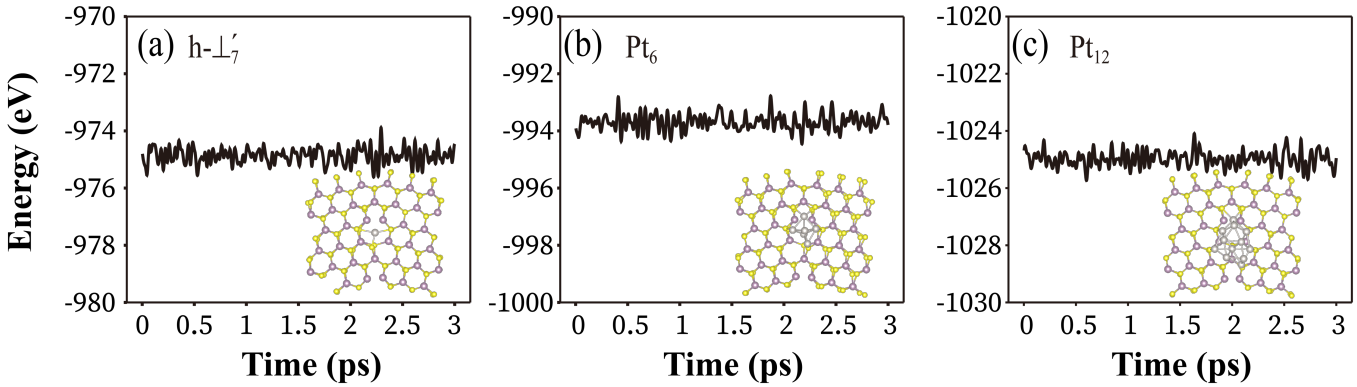

Fig. S1 Total energy as a function of time from ab initio molecular dynamics of simulation at 300 K for most stable configuration of Pt_1, Pt_6 and Pt_{12}. Corresponding atomic geometries after molecular dynamics simulation for three ps are shown in the insets.

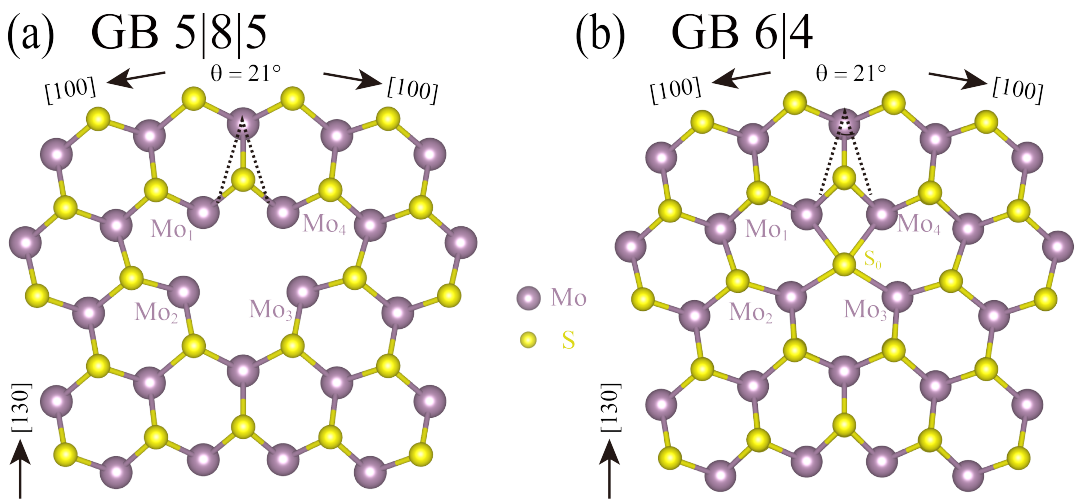

Fig. S2 Grain boundary models with 5|8|5 and 6|4 core are shown in (a) and (b), respectively.

References

1. Wu, S. Q.; Ji, M.; Wang, C. Z.; Nguyen, M. C.; Zhao, X.; Umemoto, K.; Wentzcovitch, R. M.; Ho, K. M., An adaptive genetic algorithm for crystal structure prediction. *J Phys Condens Matter* **2014,** *26* (3), 035402.

2. Zhao, X.; Nguyen, M. C.; Zhang, W. Y.; Wang, C. Z.; Kramer, M. J.; Sellmyer, D. J.; Li, X. Z.; Zhang, F.; Ke, L. Q.; Antropov, V. P.; Ho, K. M., Exploring the structural complexity of intermetallic compounds by an adaptive genetic algorithm. *Phys Rev Lett* **2014,** *112* (4), 045502.

3. Zhao, X.; Shu, Q.; Nguyen, M. C.; Wang, Y. G.; Ji, M.; Xiang, H. J.; Ho, K. M.; Gong, X. G.; Wang, C. Z., Interface Structure Prediction from First-Principles. *J Phys Chem C* **2014,** *118* (18), 9524-9530.

4. Daw, M. S.; Baskes, M. I., Semiempirical, Quantum Mechanical Calculation of Hydrogen Embrittlement in Metals. *Physical Review Letters* **1983,** *50* (17), 1285-1288.

5. Banerjea, A.; Smith, J. R., Origins of the universal binding-energy relation. *Phys Rev B Condens Matter* **1988,** *37* (12), 6632-6645.

6. Plimpton, S., Fast Parallel Algorithms for Short-Range Molecular Dynamics. *J Comput Phys* **1995,** *117* (1), 1-19.

7. Ercolessi, F.; Adams, J. B., Interatomic Potentials from 1st-Principles Calculations - the Force-Matching Method. *Europhys Lett* **1994,** *26* (8), 583-588.

8. Brommer, P.; Gahler, F., Potfit: effective potentials from ab initio data. *Model Simul Mater Sc* **2007,** *15* (3), 295-304.

9. John P. Perdew, K. B., Matthias Ernzerhof, Generalized Gradient Approximation Made Simple. *Physical review letters* **1996,** *77* (18), 4.

10. Blochl, P. E., Projector augmented-wave method. *Phys Rev B* **1994,** *50* (24), 17953-17979.

11. Kresse, G.; Joubert, D., From ultrasoft pseudopotentials to the projector augmented-wave method. *Phys. Rev. B* **1999,** *59* (3), 1758-1775.

12. Mills, G.; Jonsson, H.; Schenter, G. K., REVERSIBLE WORK TRANSITION-STATE THEORY - APPLICATION TO DISSOCIATIVE ADSORPTION OF HYDROGEN. *Surf. Sci.* **1995,** *324* (2-3), 305-337.

13. Mills, G.; Jonsson, H., QUANTUM AND THERMAL EFFECTS IN H-2 DISSOCIATIVE ADSORPTION - EVALUATION OF FREE-ENERGY BARRIERS IN MULTIDIMENSIONAL QUANTUM-SYSTEMS. *Phys. Rev. Lett.* **1994,** *72* (7), 1124-1127.

14. Henkelman, G.; Jónsson, H., Improved tangent estimate in the nudged elastic band method for finding minimum energy paths and saddle points. *J. Chem. Phys.* **2000,** *113* (22), 9978-9985.

15. Henkelman, G.; Uberuaga, B. P.; Jónsson, H., A climbing image nudged elastic band method for finding saddle points and minimum energy paths. *J. Chem. Phys.* **2000,** *113* (22), 9901-9904.

16. Maintz, S.; Deringer, V. L.; Tchougreeff, A. L.; Dronskowski, R., LOBSTER: A Tool to Extract Chemical Bonding from Plane-Wave Based DFT. *Journal of Computational Chemistry* **2016,** *37* (11), 1030-1035.

17. Maintz, S.; Deringer, V. L.; Tchougréeff, A. L.; Dronskowski, R., Analytic projection from plane-wave and PAW wavefunctions and application to chemical-bonding analysis in solids. *Journal of Computational Chemistry* **2013,** *34* (29), 2557-2567.

18. Hughbanks, T.; Hoffmann, R., Chains of trans-edge-sharing molybdenum octahedra: metal-metal bonding in extended systems. *Journal of the American Chemical Society* **1983,** *105* (11), 3528-3537.

19. Dronskowski, R.; Bloechl, P. E., Crystal orbital Hamilton populations (COHP): energy-resolved visualization of chemical bonding in solids based on density-functional calculations. *The Journal of Physical Chemistry* **1993,** *97* (33), 8617-8624.

20.Görne, A. L.; Dronskowski, R., Covalent bonding versus total energy: On the attainability of certain predicted low-energy carbon allotropes. *Carbon* **2019,** *148*, 151-158.